

Excellence in Chemistry Research

Announcing our new flagship journal

- Gold Open Access
- Publishing charges waived
- Preprints welcome
- Edited by active scientists



Meet the Editors of *ChemistryEurope*



Luisa De Cola

Università degli Studi
di Milano Statale, Italy



Ive Hermans

University of
Wisconsin-Madison, USA



Ken Tanaka

Tokyo Institute of
Technology, Japan

Accepted Article

Title: Double Hook Perylene Diimide as a New Receptor for PAHs: An Experimental and Theoretical Study

Authors: Nadia Alejandra Rodriguez-Urbe, Rodrigo Contreras-Martínez, Everardo Jaime-Adán, María Luisa García-Betancourt, Margarita I Bernal-Uruchurtu, and Carolina Godoy-Alcantar

This manuscript has been accepted after peer review and appears as an Accepted Article online prior to editing, proofing, and formal publication of the final Version of Record (VoR). The VoR will be published online in Early View as soon as possible and may be different to this Accepted Article as a result of editing. Readers should obtain the VoR from the journal website shown below when it is published to ensure accuracy of information. The authors are responsible for the content of this Accepted Article.

To be cited as: *ChemPhysChem* **2023**, e202300071

Link to VoR: <https://doi.org/10.1002/cphc.202300071>

Double Hook Perylene Diimide as a New Receptor for PAHs: An Experimental and Theoretical Study

Nadia Alejandra Rodríguez-Uribe, Rodrigo Contreras-Martínez, Everardo Jaime-Adán Dr.,
María Luisa García-Betancourt Dr., Margarita I. Bernal-Uruchurtu Prof.* and Carolina
Godoy-Alcántar Prof.*

Centro de Investigaciones Químicas, IICBA, Universidad Autónoma del Estado de
Morelos, Av. Universidad 1001, Col. Chamilpa, Cuernavaca Morelos, 62209, México.

mabel@uaem.mx (<https://www.ciquaem.mx/bernal-uruchurtu-margarita-isabel>),

cga@uaem.mx (<https://www.ciquaem.mx/godoy-alcantar-carolina>)

Abstract

In a one-step reaction, we prepared a dibenzylamine perylene diimide derivative (PDI). Its double hook structure allows for self-association with a constant of $K_d \sim 10^8 \text{ M}^{-1}$ determined by fluorescence. We confirmed its ability to bind PAHs using UV/Vis, fluorescence, and ^1H NMR titrations in CHCl_3 . The complex formation signature in UV/vis is a new band at 567nm. The calculated binding constants ($K_a \sim 10^4 \text{ M}^{-1}$) follow the trend pyrene > perylene > phenanthrene > naphthalene > anthracene. Theoretical modeling of these systems using DFT $\omega\text{B97X-D/6-311G(d,p)}$ proved helpful in rationalizing the complex formation and the observed association trend. The distinctive signal in UV/vis is due to a charge transfer in the complex from orbitals in the guest to the host. SAPT(DFT) confirmed that the driving forces in the complex formation are exchange and dispersion ($\pi-\pi$ interactions). Still, the recognition ability depends on the electrostatic component of the interaction, a minoritarian fraction.

Introduction

Polycyclic aromatic hydrocarbons (PAHs) are compounds of carbon and hydrogen organized in different numbers of fused aromatic rings. PAHs are uncharged, nonpolar, with delocalized electrons in their aromatic rings, which confer characteristic properties. PAHs are ubiquitous environmental pollutants generated primarily during the incomplete combustion of organic materials. However, emissions from anthropogenic activities are also significant, as well as those from natural sources such as petroleum or coal deposits and volcanic activities. Many PAHs have toxic, mutagenic, and carcinogenic properties.^[1] Abdel-Shafy and Mansour, in their review, discuss the PAHs' impact of these compounds on the environment and the risks to human health.^[1]

The separation, identification, and monitoring of PAHs have been carried out principally by chromatographic methods.^[2,3] In addition, new methodologies have been developed in the solid phase^[4] as porous surfaces^[5] and imprinted polymers,^[6] among others. It is possible to find alternatives to remove PAHs from the environment safely. Methods using adsorbents,^[7] bioremediation,^[1] and electro-remediation^[8] are already available.

Furthermore, some ligands able to recognize PAHs in solution have appeared in recent years. Some of these rely on the donor-acceptor concept using derivatives of boron or pyridine, for which calculated the binding constants.^[9] Another approximation considers a binuclear complex of rhenium (I) with substituents like pincers, able to recognize PAHs in solution through charge transfer and CH- π interactions.^[10] In 2004, Sánchez-Cortés group used the calix[4]arenes with different substituents in the lower rim for the selective recognition of PAHs, detecting the complexes with Surface-Enhanced Raman Scattering (SERS) spectroscopy.^[11] Their study showed that pyrene exhibits the highest specificity due to π - π stacking interaction.

The design of hosts with cage structure is also an attractive alternative because it is possible to modify the cage size and the nature of the substituents. Examples of such designs are cases like the octa-cationic cage host that encapsulates PAH as large as coronene.^[12] Also, the hosts Ex box^[13] and Ex cage^[14] exhibit significant and selective binding to PAHs among these hosts.

Perylene tetracarboxylic diimide (PDI) is a rigid planar molecule with two imide positions. PDI and its derivatives constitute a class of high-grade dyes and stable *n*-type (electron acceptor) semiconductor materials with excellent electron affinity and strong optical stability.

These characteristics allow them to form supramolecular aggregates via π - π stacking,^[15] which can have interesting optical features useful in designing optical sensors.^[16, 17] In 2020 Zang and collaborators published a review^[18] of PDI-based fluorescent and colorimetric sensors. Some of these have detected nitroaromatic compounds, nevertheless, their use for PAHs has not been explored yet. However, it has been reported that a donor-acceptor fluorescent cocrystal formed by a PDI and coronene^[19] in which π - π interactions stabilized the coronene.

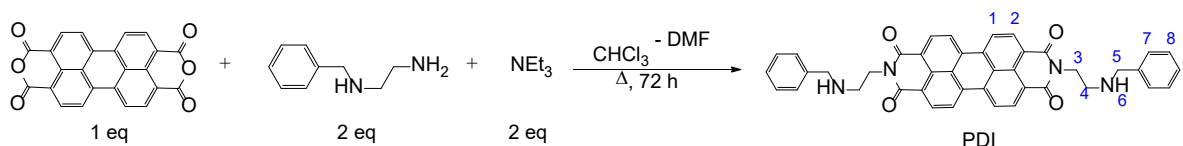
In this work, we present the synthesis of a new receptor based on perylene diimide. The characterization includes spectroscopic, photophysical, and physical analysis in solution and solid phase. Using UV/Vis, fluorescence, and ¹H NMR titrations, we studied the ability of this new receptor to bind PAHs like naphthalene, anthracene, phenanthrene, pyrene, and perylene, and calculated their binding constants. The quantum mechanical DFT studies of PDI and its PAHs complexes confirmed their interaction and the effect of the complexation in the electronic structure. Computation of their interaction energies using the rigorous symmetry-adapted perturbation theory (SAPT) allows us to provide a rationale for the measured binding constants. The Non-Covalent Interaction (NCI) Index mapped in isosurfaces shows interaction regions between PDI and PAH. FESEM images of PDI and its complexes let us see the morphological changes resulting from the complex PDI-PAH formation at a microscopic level.

Results and Discussion

Synthesis, Spectroscopic, Photophysical, and Physical Characterization of PDI

Scheme 1 shows the one-step condensation reaction leading to PDI formation. After 72 h, we recovered a purple solid soluble in CHCl₃ and THF, with 85 % yield. Its absorption and emission spectra are shown in Figure 1. Figure 1a shows a maximum absorption of PDI at 527 nm in chloroform with $\epsilon = 50843 \pm 1049 \text{ M}^{-1}\text{cm}^{-1}$ corresponding to the π - π^* transition (Figure S1 in Supporting Information, SI). Figure 1b presents the excitation ($\lambda_{em} = 582 \text{ nm}$) and emission ($\lambda_{exc} = 530 \text{ nm}$) spectra of PDI in CHCl₃, with maxima at 495 nm and 585 nm, respectively. The quantum yield of PDI was determined as $\Phi = 0.37$, using rhodamine 6G as a reference^[20] (Figure S2 in SI). This value compares^[20] with those determined in CHCl₃ for

monomeric and oligomer derivatives of perylene and hexa(ethylene glycol) with values of 0.49 and 0.47, respectively.^[21] The low fluorescence quantum yields are due to the re-absorption of emitting photons and the self-quenching due to the intra and intermolecular interactions.^[21]



Scheme 1. Synthesis of PDI. The one-step condensation of perylene-3,4,9,10-tetracarboxylic dianhydride with two equivalents of benzyl ethylenediamine and triethylamine in a mixture of chloroform and dimethylformamide gives after 72 h at 100-120 °C in constant stir, the product PDI.

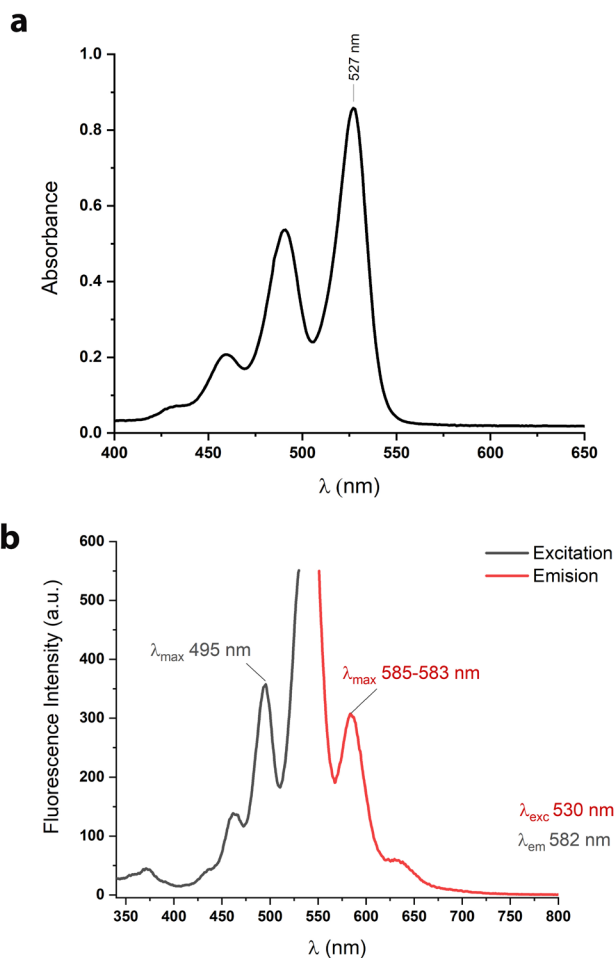


Figure 1. a. Absorption spectrum of PDI (1.5×10^{-5} M) in CHCl_3 at 25 °C. b. Partial spectra of emission ($\lambda_{\text{exc}}=530$ nm) and excitation ($\lambda_{\text{em}}=582$ nm) of PDI (2×10^{-7} M) in CHCl_3 at 25 °C.

The electrochemical characterization by cyclic voltammetry (CV) of PDI was done in acetonitrile solvent under N_2 (Figure 2). We observed the electrochemical reversibility of one electron, having the same values for the reduction and oxidation peaks. The PDI's CV recorded at various rates (Figure S3) showed no changes on the peaks. The band gap energy of PDI resulting from the HOMO and LUMO orbitals obtained from time-dependent DFT calculations using *PBE0/6-311G(d,p)* compared with the experimental electrochemical measurements appears in Table 1. The frontier orbitals are in the center of PDI, with no contributions from the substituents (Figure S20).

The agreement between theoretical and experimental results is good, with errors <1%. Furthermore, the band gap energies are close to the values reported for monomeric and oligomeric perylene diimide derivatives with hexa(ethylene glycol) in CH_2Cl_2 , 2.25 eV, and 2.24 eV, respectively,^[21] suggesting that the frontier orbitals are pretty similar to the ones of PDI.

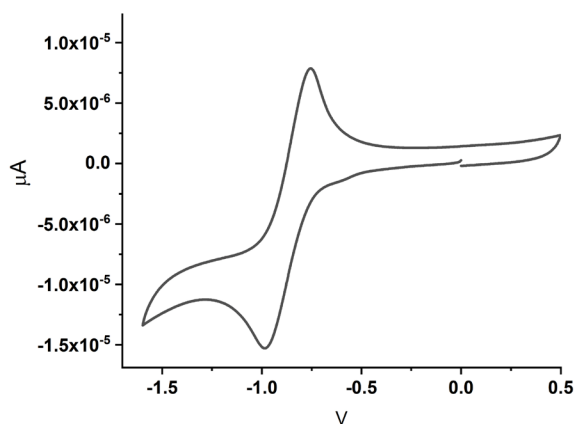


Figure 2. Cyclic voltammogram of PDI (1×10^{-3} M) in presence of tetrabutylammonium of tetrphenylborate (2×10^{-3} M) as an electrolyte and ferrocene as an intern reference in acetonitrile at 25 °C under N_2 atmosphere. Recorded at a scan rate of 60 mV/s. The oxidation peak is 12.67 μA , and the reduction peak is 12.86 μA .

Table 1. Electrochemical data of PDI from CV experiment in acetonitrile^[a] and theoretical values.

$E_g^{[b]}$ optic (eV)	Oxidation peak (A)	Reduction peak (A)	E_{onset} ox (V)	$E_{HOMO}^{[c]}$ experimental (eV)	$E_{LUMO}^{[d]}$ experimental (eV)	$\Delta E^{[e]}$ experimental (eV)	$E_{HOMO}^{[f]}$ (eV)	$E_{LUMO}^{[f]}$ (eV)	Gap [e] (eV)
2.23	12.86	12.67	-0.99	-4.22	-2.00	2.22	-6.52	-4.28	2.24

[a] Scan rate was measured at 60 mV/s; the internal reference was ferrocene, $E_{1/2ferrocene} = 0.416$ V; [b] Optic band gap, calculated from $E_g = 1240 / \lambda_{edge}$ with $\lambda_{edge} = 555$ nm from the absorbance spectra^[21, 22]; [c] $E_{HOMO} (exp) = [(E_{onset\ oxidaton} - E_{1/2ferrocene}) + 4.8]$; [d] $E_{LUMO} (exp) = E_{HOMO} (exp) + E_g$; [e] $\Delta E = E_{HOMO} - E_{LUMO}$; [f] Theoretical values calculated from the Affinity Energy (AE) and Ionization Energy (IE) of PDI using TD-DFT PBE0/6-311G(d,p). $AE = E_{LUMO} - E_{HOMO}$ and $IE = E_{HOMO}$.

In Figure 3, the absorbance spectra of PDI in solution with different solvents shows a significant solvatochromic effect. It is observed that low ϵ solvent, like THF, has the most considerable hypsochromic effect, and DMSO, high ϵ , exhibits a bathochromic one. These effects observed in the spectra do not correlate with the dielectric constant of the solvent. Fuller and Finlayson^[23] observed similar behavior and suggested that such trend could result from different degrees and mechanisms of aggregation driven by polarity changes. Therefore, low quantum yield and a high quenching correlate well with H-type assembly via $\pi-\pi$ stacking for PDI.^[15, 23]

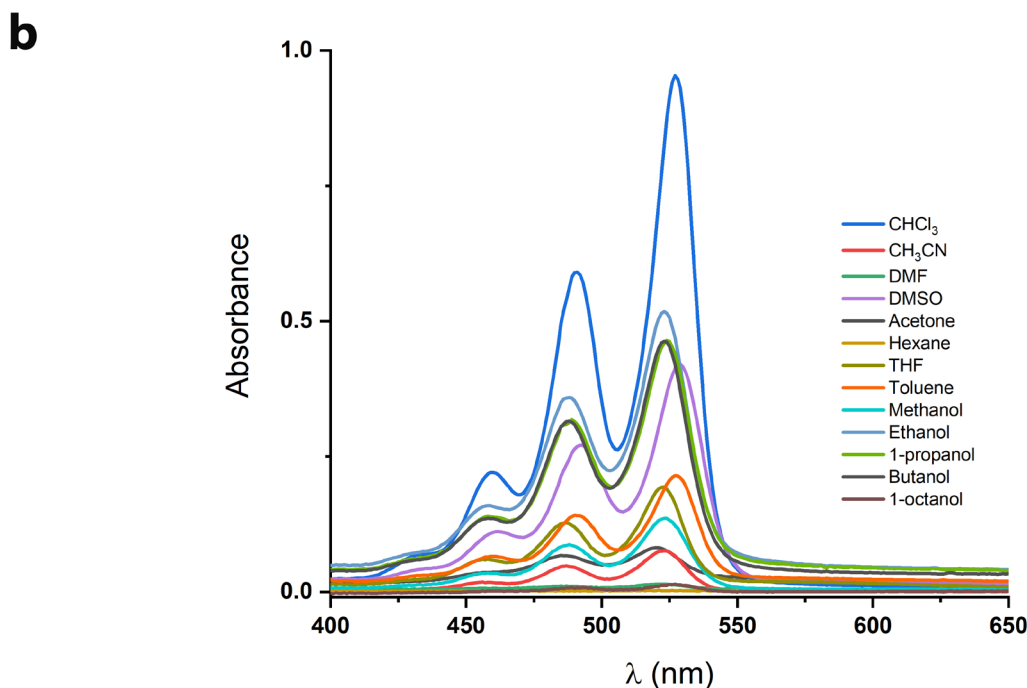
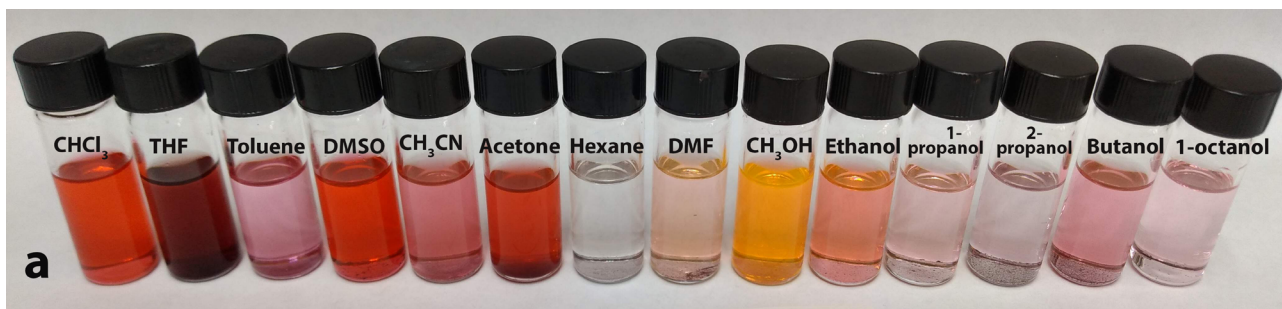


Figure 3. **a.** Color dependence of PDI (1.5×10^{-4} M) in different solvents, from left to right: CHCl_3 , THF, toluene, DMSO, CH_3CN , acetone, hexane, DMF, CH_3OH , EtOH, 1-propanol, 2-propanol, 1-butanol, and 1-octanol, **b.** Absorption spectra for some solvents. PDI is soluble in CHCl_3 and THF, slightly soluble in the other solvents shown, and not soluble in hexane.

Solid-state PDI shows characteristic wide bands, with maxima at 514 and 550 nm in the solid-state diffuse reflectance experiment. These bands correspond to the solid phase absorbance. On the other hand, fluorescence spectra in the solid state ($\lambda_{\text{exc}} = 525$ nm) show a maximum at 715 nm (Figure S5, in SI). Solid state PDI exhibits a purple-red color, with coordinates (0.22, 0.47) in the standard CIE D65 (International Commission on Illumination).^[24] The ^{13}C CP-MAS spectra illustrate the different types of groups: the aromatic

carbons at 130-120 ppm, the C=O, and aliphatic carbons at 160 and 52-37 ppm, respectively (Figure S34).

To gain further insight into PDI's geometry, we optimized its molecular structure using a density functional approximation (DFA) ω B97X-D/6-311G(d,p). Starting from different geometries, fully extended or with substituents facing each other, the results converged to a double hook-like structure, where both substituents face the perylene fragment at a 3.2 and 3.5 Å distance, with π - π interactions stabilizing this conformation (Figure 4a). To confirm the intramolecular interaction as the trigger for the doubly bent structure, we used the non-covalent interaction (NCI) index. The NCI index is a function of the electron density ρ^{el} , from which, in principle, all chemical properties can be obtained. This method uses the reduced gradient of the electronic density to confirm or discard the existence of a non-covalent interaction.^[25] The reduced density gradient (RDG) takes the form shown in equation (1):

$$s(\mathbf{r})(\mathbf{RDG}) = \frac{1}{2(3\pi^2)^{1/3}} \frac{|\vec{\nabla}\rho(\mathbf{r})|}{\rho(\mathbf{r})^{4/3}} \quad \text{Equation (1)}$$

Where $\vec{\nabla}\rho(\mathbf{r})$ is the gradient of the electronic density, and $\rho(\mathbf{r})$ is the density. Intermolecular interactions are associated with low-density and low-gradient regions; however, density and gradient alone are insufficient to discern more specific interaction types. The Laplacian of the density, $\nabla^2\rho(\mathbf{r})$, is the property that discriminates between different interactions. In particular, the sign of λ_2 (such that $\nabla^2\rho(\mathbf{r}) = \lambda_1 + \lambda_2 + \lambda_3$ with $\lambda_1 \leq \lambda_2 \leq \lambda_3$), the second eigenvalue of the electron density Hessian matrix, can distinguish attractive ($\lambda_2 < 0$) from repulsive ($\lambda_2 > 0$) interactions; when $\lambda_2 = 0$, interactions have a dispersive origin, as several studies have shown. Interactions are commonly visualized and identified using an s -vs- $\text{sign}(\lambda_2)\rho$ 2D plot; they appear as spikes in the low-gradient and low-density regions. The $\text{sign}(\lambda_2)$ helps classifying weak interactions by their relative strength. An attractive result is the 3D plot of $\text{sign}(\lambda_2)\rho$, which shows interaction regions in real space through isosurfaces. The color of the isosurface usually corresponds to the $\text{sign}(\lambda_2)\rho$; blue indicates strong attractive interactions, red indicates strong repulsive interactions, and green indicates interactions with a dispersive origin.^[25,26] In Figure 4b, we show this method applied to the PDI-optimized structure, the green isosurfaces confirm the interaction between the substituents and the perylene fragment as the origin of the stability of this conformation.

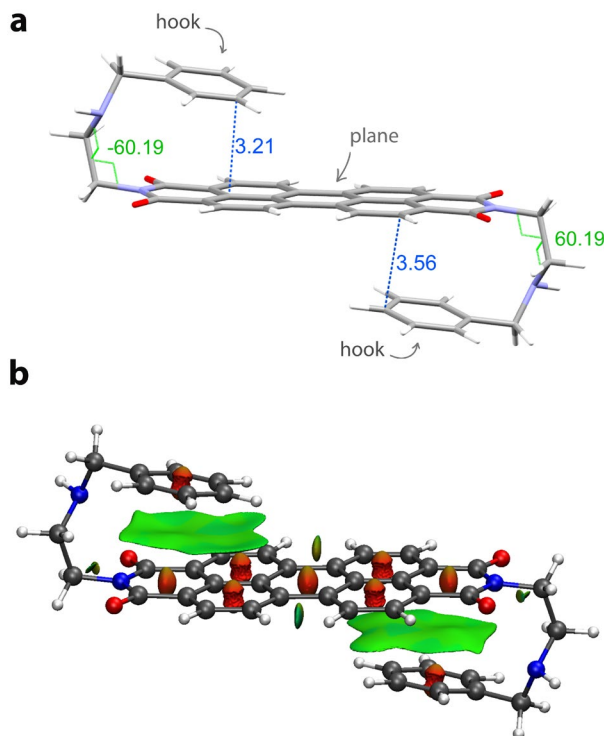


Figure 4. a. PDI optimized structure with ω B97X-D/6-311G(d,p) with SCF solvent model chloroform. The PDI plane, shows a torsion angle of 0.03° b. 3D NCI isosurfaces plot for the optimized structure of PDI.

An emission experiment with PDI at different concentrations, in chloroform and tetrahydrofuran, showed a quenching effect in both solvents as the concentration of PDI increased, suggesting a self-association behavior. However, only in tetrahydrofuran using measurements at the emission maxima, 588 nm, and the dimerization model^[27a] of equation (2):

$$I = \frac{\frac{1}{2}[PDI]I_D + (2I_M - I_D)(\sqrt{1 - 8K_d[PDI]} - 1)}{8K_d} \quad \text{Equation (2)}$$

where $[PDI]$ is the total concentration of PDI, I_D and I_M are fluorescence intensity given for dimer and monomer, and K_d is the dimerization constant (M^{-1}), we obtained a dimerization constant of $K_d = 1.2 \times 10^8 \pm 5 \times 10^6 M^{-1}$ (Figure 5a, spectra in Figure S4). This K_d agrees with values reported^[28] in methylcyclohexane ($10^7 M^{-1}$) for perylene diimides derivatives with larger groups on the imide position than PDI.

To explore the possible arrangements of PDI molecules as a dimer, we optimized it using ω B97X-D/6-31G. Starting from different possible structures, we found that the most stable conformation is the parallel symmetrical assembly of PDI. The optimal structure, shown in Figure 5b, has intramolecular distances of 3.35 to 3.37 Å and intermolecular distances of 3.35 Å. The layout of the dimer suggests the possibility of growing nanostructures by adding molecules repeating the same pattern. Despite numerous essays, it was impossible to obtain a good-quality monocrystal to confirm the length of the PDI ensembles.

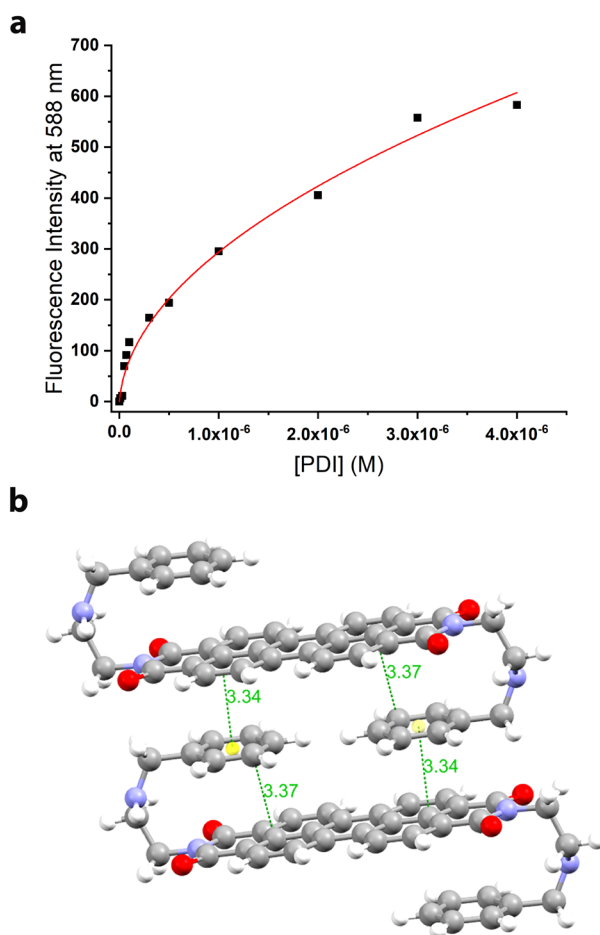


Figure 5. a. Concentration dependence of fluorescence intensity at 588 nm of PDI in THF. The solid line is the fitting curve by equation (2). b. Model of PDI dimer optimized with DFT ω B97X-D/6-31G, showing the intra e intermolecular distances.

We recorded the field emission scanning electron microscopy (FESEM) images of PDI to further characterize the solid. These gave us detailed morphological information about its crystallization course. In the first stage, the nucleation, we observed spheres in the range 290-430 nm. Considering the size of a single molecule, these would correspond to hundreds of molecules (Figure 6a). In the following steps, these spheres coalesce in sheets or layers in the condensation phase (Figure 6b-c), which finally stacks into a crystal-like object (Figure 6d).

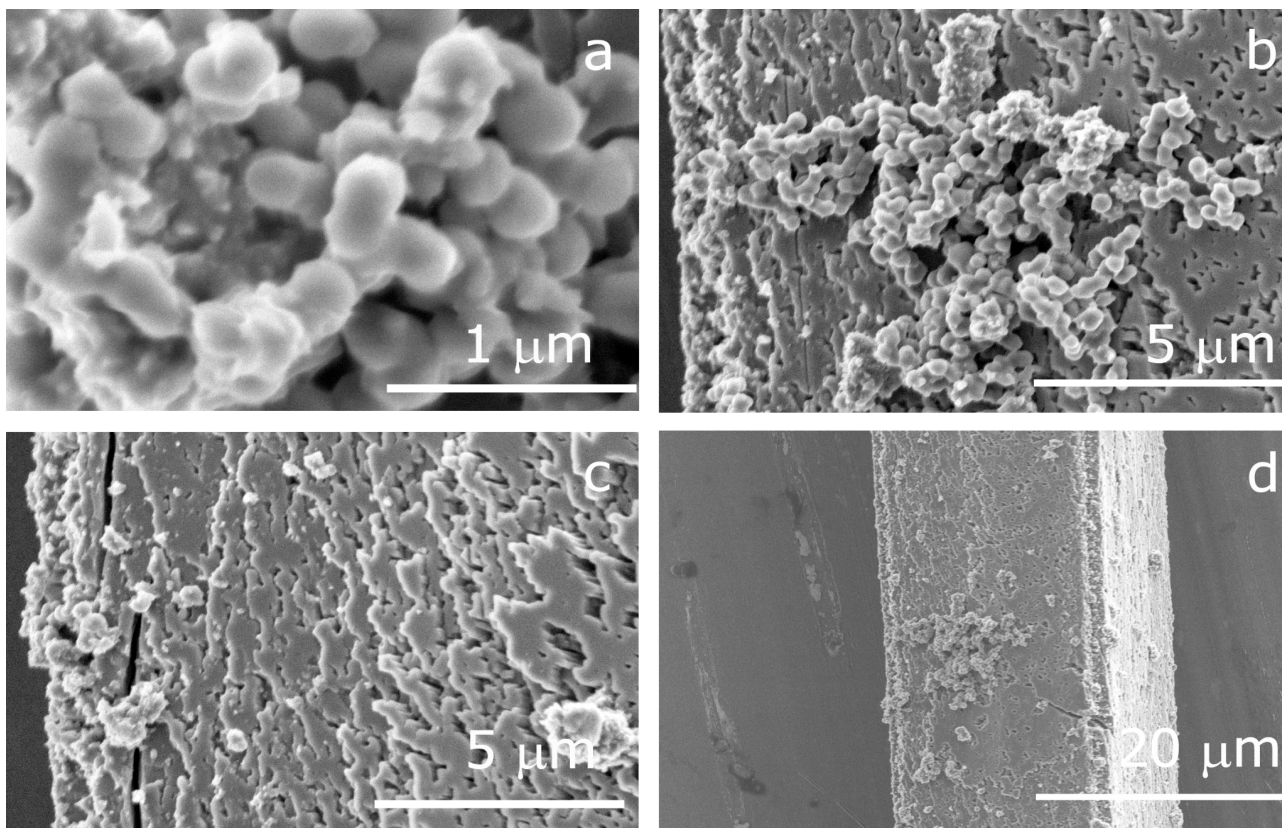


Figure 6. FESEM images of a needle crystal of PDI. **a.** Spheres with an average diameter of 290-430 nm. **b.** In this image, the single count of spheres goes up to 93. **c.** Another view of the same crystal shows layers. **d.** Side of the crystal of PDI where **a**, **b** and **c** are amplifications.

Molecular Recognition Studies

We explored the interaction between PDI and five PAHs: naphthalene, phenanthrene, anthracene, pyrene, and perylene, with titration experiments in chloroform tracked by UV/Vis, fluorescence, and ^1H NMR.

A typical titration of the PDI-perylene interaction by UV/Vis spectroscopy is shown in Figure 7a. As the concentration of the guest increases in solution, the absorbance intensity decreases at the maxima 491 and 527 nm. In addition, two isosbestic points at 480 and 535 nm pointed out the equilibrium between free species and a single complex formed. This behavior was also observed for the other PAHs. In all host-guest pairs, a new band centered at 567 nm increases proportionally to the PAH concentration; we will address the nature of this band below. From the five guests, only the titration with perylene exhibits a color change, from a pale-rose solution to a yellow one, that is also fluorescent under UV light (365 nm) (Figure 7c).

The data in the absorbance at 567 nm plot corrected by guest's absorption, and dilution vs. guest concentration (Figure 7b) was fitted to the model in equation (3)^[27b, 29]; a model that considers a 1:1 PDI-PAH complex stoichiometry for all PAHs except naphthalene. For this latter, a model with 1:2 stoichiometry resulted in a better fit. Job's experiments confirmed the PDI-PAH ratios (Figure S6, S7). Table 2 summarizes the binding constants calculated with all PAHs. The fitting profiles for the rest of the guests studied (Figure S7-S10) can be found in SI.

$$A_{obs} = A_0 + 0.5 \left(\frac{\Delta A}{[PDI]} \right) \left([PDI] + [G] + \frac{1}{K_a} - \sqrt{\left([PDI] + [G] + \frac{1}{K_a} \right)^2 - 4[PDI][G]} \right) \quad \text{Equation (3)}$$

Where $\Delta A = A_f - A_0$, A_0 , and A_f are the initial and final absorbance, $[PDI]$ and $[G]$ are the concentrations of PDI (1.5×10^{-5} M) and of the guest added, and K_a is the association constant.

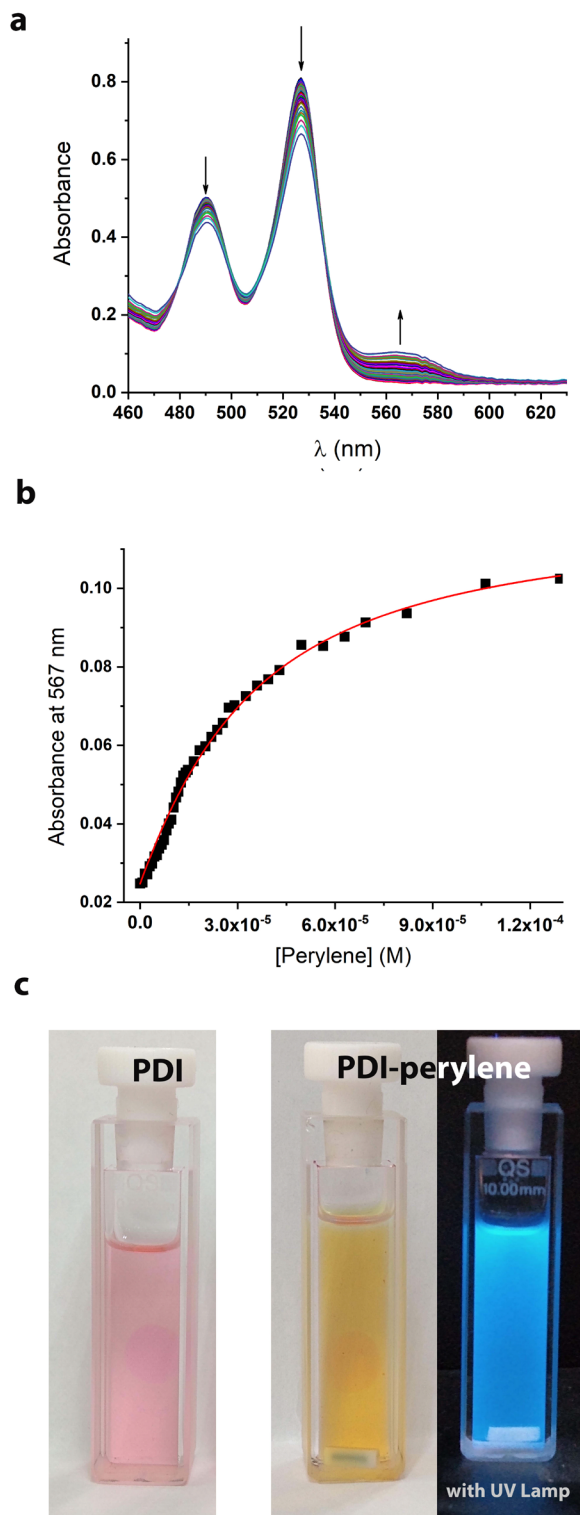


Figure 7. a. UV/Vis spectrophotometric titration spectra of PDI (1.5×10^{-5} M) with perylene in CHCl_3 at 25 °C. Arrows indicate the direction of the change in absorbance b. Titration plot at 567 nm. Solid line is the theoretical

profile calculated with equation (3). **c.** PDI solution before and after perylene addition, and under UV light ($\lambda = 365$ nm).

Figure 8a shows the fluorescence changes during the titration of PDI with perylene at $\lambda_{\text{exc}}=530$ nm. Adding the guest solution produces a hypsochromic effect and a fluorescence quench at the 585 nm maximum. The data of fluorescence intensity at 585 nm vs. guest concentration (Figure 8b) was fitted with equation (4)^[27c] which corresponds to a model that considers a 1:1 PDI-PAH stoichiometry. The resulting binding constants are presented in Table 2. The SI includes equivalent plots (Figure S11-S14) for the rest of the studied guests.

$$\Delta I = \Delta i \left(\frac{[PDI] + [G] + \frac{1}{K_a}}{2} \right) - \sqrt{\left(\frac{[PDI] + [G] + \frac{1}{K_a}}{2} \right)^2 - [PDI][G]} \quad \text{Equation (4)}$$

Where ΔI is the change in fluorescence intensity, $\Delta i = i_{PDI-G} - i_{PDI}$ is the difference of intrinsic molar fluorescence, $[PDI]$ and $[G]$ are the concentration of PDI (2×10^{-7} M) and the guest added, and K_a is the association constant.

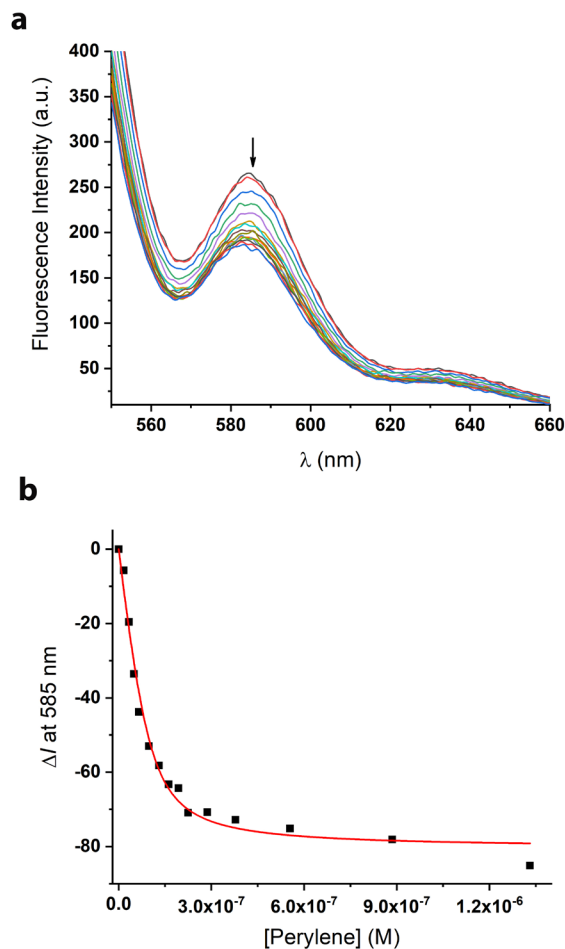


Figure 8 a. Fluorescence titration with $\lambda_{exc}=530$ nm of PDI (2×10^{-7} M) with perylene in CHCl_3 at 25°C , arrow indicates the quench in fluorescence intensity **b.** Titration plot at 585 nm, solid line is the theoretical profile calculated with equation (4).

The ^1H NMR titration of PDI with perylene is shown in Figure 9. Adding 0.25 to 3 equivalents of perylene to the PDI solution induces an up-field shift of protons 1 and 2, assigned to the PDI fragment due, to a shielding effect on the guest through $\pi-\pi$ interactions. Titration experiments of the other guests show the same effect. Nonetheless, perylene causes the largest $\Delta\delta_{\text{H}1}$: 0.328 ppm, and $\Delta\delta_{\text{H}2}$: 0.508 ppm; followed by pyrene: $\Delta\delta_{\text{H}1}$: 0.289 ppm and $\Delta\delta_{\text{H}2}$: 0.259 ppm, phenanthrene: $\Delta\delta_{\text{H}1}$: 0.095 ppm and $\Delta\delta_{\text{H}2}$: 0.155 ppm, naphthalene: $\Delta\delta_{\text{H}1}$: 0.025 ppm and $\Delta\delta_{\text{H}2}$: 0.054 ppm, and anthracene: $\Delta\delta_{\text{H}1}$: 0.026 ppm and $\Delta\delta_{\text{H}2}$: 0.050 ppm. As shown in Figure 9, aliphatic protons 3, 4, and 5 have no noticeable change.

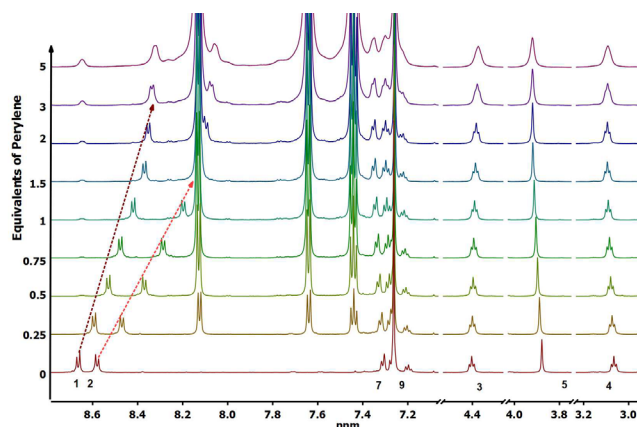


Figure 9. ^1H NMR titration of PDI (1×10^{-2} M) with different equivalents of perylene in CDCl_3 , 600 MHz at 25°C . Numbers under signals correspond to the PDI protons according to Scheme 1. Red arrows indicate the direction of the displacement change in protons 1 and 2.

Table 2 summarizes all the binding constants for PDI-PAH calculated in this work and their comparison with other hosts reported in the literature. The binding constants calculated by UV/Visible spectroscopy at $\lambda=567$ nm are $\approx 10^4$ M^{-1} , with an error below 10%, showing the trend: pyrene > perylene > phenanthrene > naphthalene > anthracene. On the other hand, in fluorescence at $\lambda=585$ nm binding constants span from 10^6 to 10^7 M^{-1} ; ordered as: perylene > pyrene \cong anthracene > naphthalene > phenanthrene. Although ^1H NMR titration experiments did not allow to calculate the binding constants; the change in the chemical shifts, $\Delta\delta$, suggests the affinity of PDI for PAH. Thus, the tendency observed: perylene > pyrene > phenanthrene \cong naphthalene > anthracene coincides with the UV/Vis trend. It is important to emphasize that the trends obtained are crucially dependent on the methodology employed, the PDI concentration used, its high self-association constant, and therefore the different ratios of monomeric/dimeric forms present in the solution.

The UV/Vis determined binding constants of other hosts aimed to selectively bind PAHs (Table 2) are of the same magnitude, 10^4 M^{-1} , as the values found for PDI in this work. However, with fluorescence all PDI's binding constants are greater than those previously reported.

Table 2. Binding constants (K_a , M^{-1}) calculated in this work for PDI-PAH (1:1) complexes in $CHCl_3$ and their comparison with other hosts.^[a]

This work	Naphtalene	Anthracene	Phenanthrene	Pyrene	Perylene
UV/vis (567 nm)	$3.6 \times 10^4 \pm 6 \times 10^3$ K_2 1.8×10^5 ^[b]	$3.04 \times 10^4 \pm 4 \times 10^3$	$3.8 \times 10^4 \pm 3 \times 10^3$	$5.11 \times 10^4 \pm 2 \times 10^3$	$4.02 \times 10^4 \pm 3 \times 10^3$
Fluorescence (585 nm)	$1.9 \times 10^7 \pm 3 \times 10^6$	$2.93 \times 10^7 \pm 7 \times 10^6$	$3.4 \times 10^6 \pm 8 \times 10^5$	$2.98 \times 10^7 \pm 4 \times 10^6$	$4.7 \times 10^7 \pm 9.6 \times 10^6$
Reference (solvent)					
[9] (EtOH)	2.9×10^4 ^[c]	8.8×10^4 ^[c]	6.6×10^4 ^[c]	-	-
[13] ($CHCl_3$, CH_3CN)	-	8.8×10^2 ^[d]	1.38×10^3 ^[e]	7.16×10^3 ^[e] 1.01×10^4 ^[d]	8.81×10^4 ^[d]
[12] (CH_3CN)	2.1×10^2 ^[d]	1.39×10^4 ^[e]	-	1.99×10^4 ^[e]	-
[14] (CH_3CN)	2.82×10^3 ^[e]	-	6.22×10^4 ^[e]	6.77×10^5 ^[e]	5.54×10^6 ^[e]
[30] ($CHCl_3$)	8.0 ^[d]	1.23×10^2 ^[d]	42.6 ^[d]	-	-
[10] (CH_2Cl_2)	1.4×10^4 ^[f]	2.1×10^4 ^[f]	1.8×10^4 ^[f]	1.3×10^4 ^[f]	-

[a] See chemical structures in Table S1; [b] K_2 (M^{-2}) calculated for PDI:2 naphthalene complex. Both K 's calculated at 527 nm; [c] K calculated using UV/vis spectroscopy; [d] K calculated by RMN; [e] K calculated with ITC (Isothermal titration calorimetry); [f] K calculated by fluorescence.

The images in Figure 10 show the FESEM analysis of PDI-PAH complexes in which a severe change in morphology from the original PDI and that of the guests is observed (Figure S19). It is possible to see a significant flattening of the original spheres, and the extent of the change correlates with the size of the PAH guest. For example, the particles agglomerate into rodlike nanostructures on the PDI-perylene complex. These changes might arise from the perturbation PAH guest provokes on the self-association of PDI.

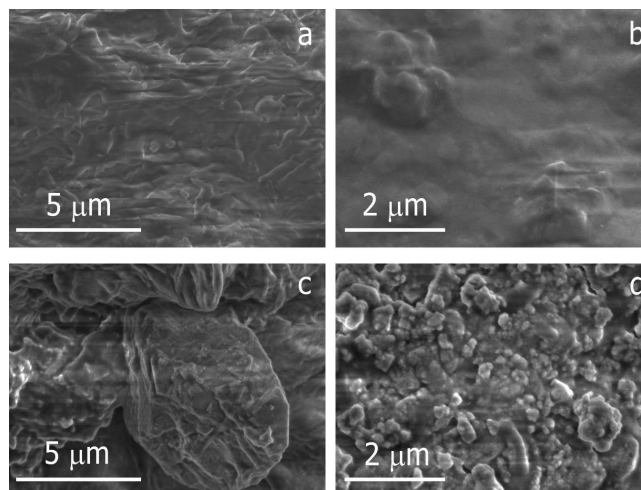


Figure 10. FESEM images of the PDI-PAH studied in this work: **a.** PDI-naphthalene, **b.** PDI-phenanthrene, **c.** PDI-pyrene and **d.** PDI-perylene. See details in text.

Molecular Modeling Studies

Initial efforts to optimize the structure of the PDI-PAH complexes with *B3LYP* functional^[31-33] were unsuccessful, indicating the need for dispersion-corrected DFA. For this reason, we optimized all the PDI-PAH complexes using ω *B97X-D*^[34] with the *6-311G(d,p)* basis set. First, an unrelaxed scan of the PAH-PDI distance helped us to identify how close the molecules need to be to stabilize the complex, and then we performed a complete optimization starting from that point. The optimized structure in the model solvent (CHCl_3) is indistinguishable from that in vacuo. The optimal geometry of the perylene-PDI complex appears in Figure 11. The perylene molecule lays above PDI's plane, and the distance between the centroids of the guest and the host is 3.46 Å; this value falls in the range for stable π - π complexes.^[35] It is possible to observe that one PDI's hooks of PDI rotates to reduce the repulsion between the protons of both fragments. The other hook reduces its intramolecular distance to compensate for the effect caused by the guest molecule. Structures for the rest of the PDI-PAH complexes (Figures S21-S24) are quite similar, *i.e.*, the guest is placed over the plane of PDI with distances ranging from 3.2 to 3.7 Å, larger than in the PDI-perylene complex. Upon complexation, a significant loss of planarity occurs in the host. The most significant distortion happens with perylene, where a 19.5° angle forms. PDI's plane distortion in the other complexes is smaller than in PDI-perylene, ranging from 5.3 to 10.3°. The PDI distortion results from the 1:1 stoichiometry; in the 1:2 PDI-

naphthalene (Figure S24d), where the guest molecules occupy both faces of the PDI plane, only a tiny distortion occurs, 5.5° . Since the guest-host distance of naphthalene is similar in the 1:1 and the 1:2 complex, 3.3-3.5 Å, but the distortion angle reduces from 10.3° to 5.5° , the loss of the planarity can be attributed to the distinct electronic density on both sides of PDI's plane.

The interaction between PDI and PAH molecules significantly affects their electronic structure and spectroscopic properties. The TD-DFT *PBE0/6-311G(d,p)* calculation of the excited states of the PDI-perylene complex showed that the LUMO orbital is on PDI and the HOMO on the perylene guest; this results in a charge-transfer complex (Figure 11). The HOMO←LUMO transition matches the growing band at 567 nm previously described. Upon complexation PDI's HOMO and LUMO are blue-shifted, whereas the guest's frontier orbitals do not change. For this reason, the HOMO-1←LUMO and HOMO-2←LUMO at 527 and 491 nm, respectively, are not of charge-transfer bands but the original PDI's absorption ones.

Anthracene and pyrene also form charge-transfer complexes. In contrast, phenanthrene and naphthalene do not; both orbitals, HOMO and LUMO, rest on the PDI molecule (see Figures S21-S24). However, for these last couple of PAHs, the 567 nm band comes from a charge transfer occurring from HOMO-1←LUMO transitions.

The trend of the calculated energy gaps, PDI-perylene (3.40 eV) > PDI-anthracene (3.96 eV) > PDI-pyrene (4.23 eV) > PDI-phenanthrene (5.13 eV) > PDI-naphthalene (5.21 eV), do not match the previously discussed UV/vis K_a trend, except on the extremes.

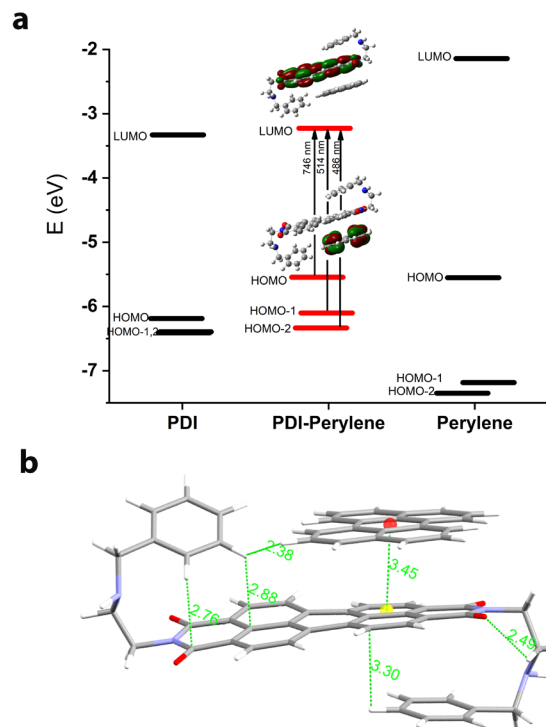


Figure 11. a. Energy plot of frontier molecular orbitals for PDI, perylene and its complex PDI-perylene calculated with *TD-DFT PBE0/6-311G(d,p)* density functional approximation.^[36] b. Optimized structure of PDI-perylene complex obtained from *ωB97X-D/6-311G(d,p)* with SCF solvent model chloroform.

We calculated the PDI-PAH complexes' interaction energy (IE) using two different approaches (see Table 3). One of them is the supermolecular method (SM), which allows us to include the solvent effect in this term. The other, SAPT(DFT), is a theory that, from the exact calculation of the meaningful terms for the interaction, the electrostatic, induction, exchange, and dispersion components compute the total interaction energy.^[37,38] It is well known that the dispersion component, from quantum origin, represents a significant challenge for intermolecular interaction studies. Moreover, most DFAs severely underestimate dispersion. Thus, the need for an empirically corrected functional; *ωB97X-D* is one of such corrected functionals; it captures a reasonable fraction of this contribution.^[39,34] SAPT(DFT) interaction energies are generally as good as wavefunction CCSD(T) energies,^[38b] which for the complexes studied here, is not a feasible option.

The supermolecular interaction energies (SM IEs) suggest a more significant interaction, 20-40% larger than SAPT(DFT). This difference is an artifact of the SM approach used with

DFA. Some authors have probed that this is due to factors like the basis set superposition error present in SM and not in SAPT(DFT).^[38b]

SAPT(DFT) confirmed that dispersion and exchange are the most significant contributions to the interaction, almost 80% of the total E_{int} , a signature of π - π interactions. The empirical dispersion corrections rely on the distance between the interacting centers, and in these extended π fragments, they tend to overcorrect, *i. e.*, to overestimate the interaction energy. Given this situation, SAPT(DFT) E s are better suited for this study.

The dissection of the interaction energies on electrostatic terms: electrostatic and induction, and those of quantum origin: dispersion, and exchange showed that the K_a trend matches with the electrostatic tendency (pyrene >> perylene > phenanthrene > naphthalene > anthracene). Albeit the electrostatic fraction is minoritarian, it suffices to differentiate the guest's affinity for PDI.

Table 3. Interaction energies computed for five PDI-PAH complexes with two different approaches and SAPT(DFT) components (see details in text).

PDI-PAH complex	E_{int} (kJ/mol)		SAPT(DFT) E_{int} components (kJ/mol)			
	SM	SAPT(DFT)	Electrostatic	Induction	Exchange	Dispersion
Naphthalene	-67	-48	-21.7	-9.2	57.9	-74.9
Anthracene	-85	-61.3	-28.2	-13	75.5	-95.6
Phenanthrene	-85.2	-70.9	-29.4	-12.4	76.3	-105.4
Pyrene	-93	-66.4	-32.7	-13.9	86.3	-106.1
Perylene	-104.8	-79.2	-38.4	-16.2	102.7	-127.4

To gain a further understanding of the extend of forces governing the recognition between PDI and PAHs, we employed NCIPLLOT4.^[40] Figure 12 shows the 2D and 3D plots of the NCI study for the PDI-perylene complex, where we can distinguish between the intra and intermolecular interactions. We colored the surfaces according to their origin: in blue, all the non-covalent interactions present in the complex, including the intramolecular ones, and in orange, we superposed those corresponding only to PDI-perylene (intermolecular

interactions). We want to draw attention to the surface between both H1; these correspond to an attractive hydrogen-hydrogen intramolecular interaction. These protons are those that, in the ^1H NMR titrations, are shifted up-field, indicating the shielding of such protons. The NCI study of the other complexes can be found in the SI Figures S25-S31.

An additional advantage of NCI analysis is that the value of the isosurfaces' integrals correlate with the interaction energy.^[40] The computation of the PDI-PAH isosurface integrals shows a clear correlation with the number of aromatic rings in the guest molecules, *i.e.*, the size of the PAH molecule: 1:2 PDI-naphthalene (30.13) > PDI-perylene (30.15) > PDI-pyrene (28.43) > PDI-phenanthrene (27.58) > PDI-anthracene (27.57) > PDI-naphthalene (25.86).

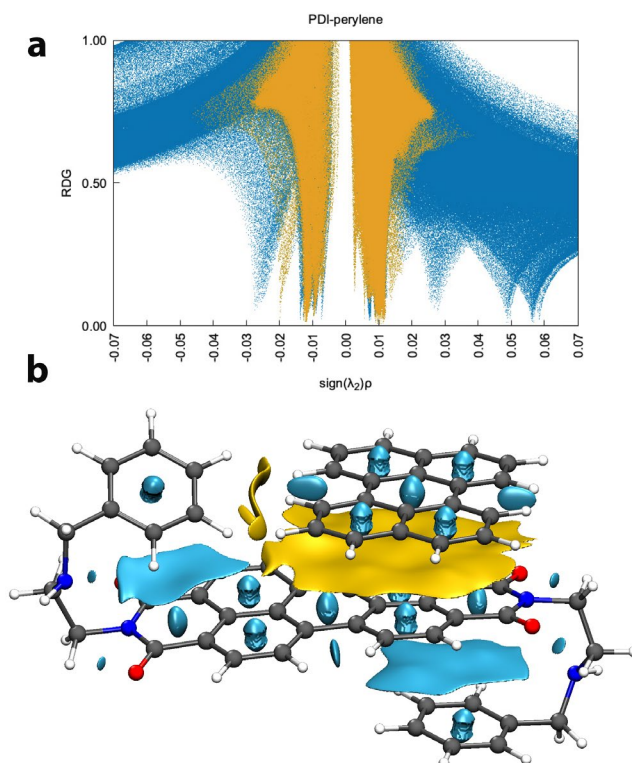


Figure 12. Standard NCI index representations for PDI-perylene complex using a promolecular density. **a.** Reduced density gradient (RDG) plotted vs. $\text{sign}(\lambda_2)\rho(\mathbf{r})$. **b.** Isosurfaces of $\text{RDG}(\mathbf{r})=0.3$ colored to distinguish inter (in yellow) and intramolecular (in blue) interactions.

Conclusions

The perylene diimide (PDI) derivative has the advantage of a straightforward preparation in a one-step reaction. The DFT studies showed that the preferred conformation is a double hook. This geometry favors a self-association process, $K_d \sim 10^8 \text{ M}^{-1}$, responsible for the sphere aggregates on a microscopic scale. In solution, the solvatochromic effect observed might be relevant for optical applications. As a receptor for PAHs, it has a similar ability to other hosts reported previously, 10^4 M^{-1} (UV/Vis) to $10^6\text{-}10^7 \text{ M}^{-1}$ (fluorescence), but with greater sensitivity with this latter method. Furthermore, the complex formation results in the appearance of a charge-transfer band at 567 nm (UV/vis titration), a feature extremely useful in sensor development. This new host proved to be of general application in detecting PAHs; however, in UV/vis, there is a slight preference for pyrene > perylene > phenanthrene > naphthalene > anthracene.

As expected, and confirmed through the theoretical study, $\pi\text{-}\pi$ interactions drive the recognition process. The most significant contribution to the E_{int} of the complexes is from quantum origin, dispersion and exchange. Still, the observed trend results from the relative electrostatic terms, electrostatic and induction, modulate the trend observed by UV/vis and NMR titrations, demonstrating how a minoritarian contribution is crucial in the thermodynamical recognition phenomena.

We are currently developing a simple solid-phase PDI sensor to remove PAHs from water.

Experimental Section

General Procedures and Methods

All reagents, including perylene-3,4,9,10-tetracarboxylic dianhydride, N-benzylethylenediamine, triethylamine, perylene, pyrene, phenanthrene, anthracene and naphthalene were commercially available and were used as received.

The **electronic absorption spectra** were recorded at 25 °C on a Hewlett–Packard 8452A diode array spectrophotometer in solution. The **reflectance diffuse** was recorded on a Cary 100. The **fluorescence spectra** were recorded at 25 °C on a Perkin Elmer LS 55 fluorimeter.

The **NMR studies** were carried out on a Bruker Avance III HD 500 MHz and a Jeol ECZ600R

600 MHz instruments. Chemical shifts (δH and δC) are given in ppm. TMS (^1H , $^{13}\text{C}=0$ ppm) were used as standard reference in CDCl_3 .

UV/Vis spectrophotometric titration experiments were carried out at 25 °C in chloroform. Aliquots of 10 – 20 μL of the guest solution (9.3×10^{-4} M) were added to the PDI solution (1.5×10^{-5} M). The spectra were recorded after each addition.

Fluorescence titration experiments were carried out by adding aliquots of 5, 10, and 20 μL of the guest solution (8.3×10^{-6} M) to the PDI solution with a given concentration of 2×10^{-7} M in chloroform at 25 °C. The spectra were recorded after each addition.

For ^1H NMR titrations, the solutions of guest and PDI were prepared in CDCl_3 . The guests' stock solutions (0.2 M) were each prepared in 200 μL of CDCl_3 and kept in constant stirring. The titrations were carried out by adding 10 μL of the guest stock solution aliquots directly to the NMR tube containing the PDI compound (1×10^{-2} M). The spectra were recorded after each addition.

Self-association experiments were carried out in tetrahydrofuran recording the fluorescence spectra ($\lambda_{\text{exc}}=530$ nm) of thirteen independent solutions of PDI, then the fluorescence at 588 nm was plotted against PDI concentration and the experimental data was fitted using the equation 2.

Quantum-yield was determined by an indirect method in CHCl_3 for PDI spectra with rhodamine 6G in ethanol as reference. The PDI absorbance values were measured at 530 nm and fluorescence spectra were recorded with $\lambda_{\text{exc}} = 530$ nm. According to protocol described in Technical Note: 52019 of Thermo Fisher Scientific^[20]. See details in Figure S2.

Cyclic Voltammetry experiments were executed in acetonitrile under N_2 . PDI (1×10^{-3} M) was previously dissolved completely in 2 mL of CHCl_3 to give a final volume of 10 mL inside the cell. We used tetrabutylammonium tetraphenylborate as an electrolyte and ferrocene as an intern reference. An Ag wire was used as a pseudo reference electrode, Pt as the counter electrode and the working electrode was of 'glassy-carbon'. The CV were recorded on a Gamry 600 Potentiostat/Galvanostat/ZRA.

Field emission scanning electron microscopy (FESEM): a drop of each of the UV/Vis spectrophotometric titration was placed and let dry on a copper film, then the image was recorded on the Hitachi SU5000 field emission scanning electron microscope.

Synthesis of PDI: 160 mg of perylene-3,4,9,10-tetracarboxylic dianhydride were put in a pressure vessel equipped with PTFE plug, then added 3 mL of DMF and 4 mL of CHCl_3 , and 124 mL of benzyl ethylenediamine (2 equivalents) in presence of 2 equivalents of

triethylamine, the vessel was sealed and put in constant stir at 100-120 °C for 72 h. The product was recovered by filtration then washed with ethanol and dried under vacuum. We obtained a dark purple reddish solid with an 85 % yield. **¹H NMR** (600 MHz, 298 K, CDCl₃): δ(ppm)= 3.067 (*t*, H4, 4H), 3.879 (*s*, H5, 4H), 4.402 (*t*, H3, 4H), 7.197 (*t*, H9, 2H), 7.281 (*m*, H8, 4H), 7.305 (*m*, H7, 4H), 8.557 (*d*, H2, 4H), 8.649 (*d*, H1, 4H). **¹³C DEPT-q** (150 MHz, 298 K, CDCl₃): δ(ppm)= 163.7 (C=O), 140.5, 134.74, 131.6, 129.5, 128.5, 128.3, 127.03, 126.53, 123.4, 123.2, 53.70 (C3), 47.15 (C5), 40.13 (C4). **IR**: ν (cm⁻¹)= 3061.9, 3030.9 (N-H); 1687.7, 1649.5, 1587.6 (C=O); 1436.5, 1345.5 (C-C); 810.4, 737.6 (C-C_{aromatic}). **HRMS FAB+**: •+M= 657 m/z. (Figures S32-S36 in SI).

Computational Details: Electronic structure calculations were performed with Gaussian09 suite of programs^[41] and PSI4v1.5^[42,43] was used for the SAPT(DFT) calculations. NCI studies were carried out with NCIPLLOT4 code^[40] using the xyz coordinates of PDI-optimized and PDI-guest (guest = naphthalene, phenanthrene, anthracene, pyrene and perylene) calculations. NCI index was calculated with fine grid and promolecular approximation^[41,42] (computed from the sum of atomic densities).

Acknowledgments

N. A. Rodriguez-Urbe acknowledges CONACyT for the scholarship (CVU No. 739329). E. Jaime-Adán acknowledges CONACyT for the fellowship 2157889 (CVU No. 365678). The authors thank Prof. Anatoly K. Yatsimirsky for contributing to the analysis of the experimental results and revision of the manuscript. The authors thank LANEM laboratory for the use of NMR spectrometers and CIICAP for the use of field scanning electron microscope.

Conflict of Interest

The authors declare no conflict of interest.

Data Availability Statement

The data that support the findings of this study are available in the Supporting Information of this article.

Keywords: perylene diimide • aromatic molecules • pi-interaction • binding constants • noncovalent interaction analysis

References

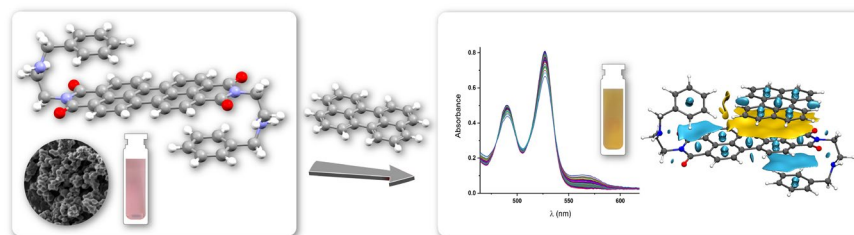
- [1] H. I. Abdel-Shafy, M.S.M. Mansour, *Egypt. J. Pet.* **2016**, *25*, 107-123.
- [2] T. Vo-Dinh, J. Fetzer, A. D. Campiglia, *Talanta* **1998**, *47*, 943-969.
- [3] S. A. Wise, L. C. Sander, M. M. Schantz, *Polycycl. Aromat. Compd.* **2015**, *35*, 1-61.
- [4] M. Rahman, Z. A. Begum, H. Hasegawa, *Microchem. J.* **2013** *110*, 485-493.
- [5] D. Bonifazi, S. Mohnani, A. Llanes-Pallas, *Chem. Eur. J.* **2009**, *15*, 7004-7025.
- [6] N. Kirsch, J. P. Hart, D. J. Bird, R. W. Luxton, D. V. McCalley, *Analyst.* **2001**, *126*, 1936-1941.
- [7] S. Ncube, L. Madikizela, E. Cukrowska, L. Chimuka, *TrAC, Trends Anal. Chem.* **2018**, *99*, 101-116.
- [8] M. Pazos, E. Rosales, T. Alcántara, J. Gómez, M. A. Sanromán, *J. Hazard. Mater.* **2010**, *177*, 1-11.
- [9] T. Chaudhuri, S. Salampuria, C. Mukhopadhyay, P. K. Tapaswi, S. Chattopadhyay, M. Banerjee, *J. Photochem. Photobiol. A Chem.*, **2012**, *22*, 55-62.
- [10] V. Sathish, M. M. Krishnan, M. Velayudham, P. Thanasekaran, K.-L. Lu, S. Rajagopal, *Spectrochim. Acta, Part A* **2019**, *222*, 117160-117166.
- [11] P. Leyton, S. Sánchez-Cortes, J. V. García-Ramos, C. Domingo, M. Campos-Valette, C. Saitz, R. E. Clavijo, *J. Phys. Chem. B.* **2004**, *108*, 17484-17490.
- [12] H. Duan, Y. Li, Q. Li, P. Wang, X. Liu, L. Cheng, Y. Yu, L. Cao, *Angew. Chem., Int. Ed.* **2020**, *56*, 2-12.
- [13] J. C. Barnes, M. Juríček, N. L. Strutt, M. Frasconi, S. Sampath, M. A. Giesener, P. L. McGrier, C. J. Bruns, C. L. Stern, A. A. Sarjeant, J. F. Stoddart, *J. Am. Chem. Soc.* **2013**, *135*, 183-192.
- [14] E. J. Dale, N. A. Vermeulen, A. A. Thomas, J. C. Barnes, M. Juríček, A. K. Blackburn, N. L. Strutt, A. A. Sarjeant, C. L. Stern, S. E. Denmark, J. F. Stoddart, *J. Am. Chem. Soc.* **2014**, *136*, 10669-10682.
- [15] S. Chen, P. Slattum, C. Y. Wang, L. Zang, *Chem. Rev.* **2015**, *115*, 11967-11998.

- [16] Q. Wang, Z. Li, D.D. Tao, Q. Zhang, P. Zhang, D.P. Guo, Y.B. Jiang, *Chem. Commun.* **2016**, 52, 12929–12939.
- [17] H. Wang, X.F. Ji, Z.T. Li, F.H. Huang, *Adv. Mater.* **2017**, 29, 1606117-1606138.
- [18] S. Chen, Z. Xue, N. Gao, X. Yang, L. Zang, *Sensors* **2020**, 20, 917-945.
- [19] C. Wang, J. Wang, Na. Wu, M. Xu, X. Yang, Y. Lu, L. Zang, *RSC Adv.* **2017**, 7, 2382–2387.
- [20] M. W. Allen, **2010**, *Measurement of Fluorescent Quantum Yields*, Technical Note: 52019, Thermo Fisher Scientific.
- [21] J. B. Bodapati, H. Icil, *Dyes Pigments* **2008**, 79, 224-235.
- [22] A. Shafiee, M. M. Salleh, M. Yahaya, *Sains Malaysiana* **2011**, 40, 173-176.
- [23] C. A. Fuller, C. E. Finlayson, *Phys. Chem. Chem. Phys.* **2017**, 19, 31781-31787.
- [24] International Commission on Illumination (CIE), 2020, Colorimetry - Part 2: CIE standard illuminants, DIS 11664-2:2020.
- [25] E. R. Johnson, S. Keinan, P. Mori-Sanchez, J. Contreras-Garcia, A. J. Cohen, W. Yang, *J. Am. Chem. Soc.* **2010**, 132, 6498-6506.
- [26] J. Contreras-García, E. R. Johnson, S. Keinan, R. Chaudret, J. P. Piquemal, D. N. Beratan, W. Yang., *J. Chem. Theory Comput.* **2011**, 7, 625-632.
- [27] a) H. Schneider, A. K. Yatsimirsky, *Principles and Methods in Supramolecular Chemistry*, John Wiley and Sons Ltd, England, **2000**, p.147, b) p. 142, c) p. 139.
- [28] Z. Chen, A. Lohr, C. R. Saha-Moller, F. Würthner, *Chem. Soc. Rev.* **2009**, 38, 564-584.
- [29] N. A. Rodríguez-Urbe, R. Pérez-González, B. E. Domínguez-Mendoza, F. Medrano, C. Godoy-Alcántar, *Inorg. Chem. Commun.* **2019**, 104, 61-70.
- [30] W. Huang, W. E. Liu, E. Valkonen, H. Yao, K. Rissanen, W. Jiang, *Chin. Chem. Lett.* **2018**, 29, 91-94.
- [31] A. D. Becke, *Phys. Rev. A.* **1988**, 38, 3098-3100.
- [32] C. Lee, W. Yang, R. G. Parr, *Phys. Rev. B*, **1988**, 37, 785-789.
- [33] A. D. Becke, *J. Chem. Phys.*, **1993**, 98, 1372-1377.
- [34] J. D. Chai, M. Head-Gordon, *Phys. Chem. Chem. Phys.* **2008**, 10, 6615-6620.
- [35] R. León-Zárate, J. Valdés-Martínez, *Cryst. Growth Des.* **2021**, 21, 3756-3769.
- [36] C. Adamo, V. Barone, *J. Chem. Phys.* **1999**, 110, 6158-6170.
- [37] A. J. Misquitta, B. Jeziorski, K. Szalewicz, *Phys. Rev. Lett.* **2003**, 91, 033201.
- [38] a) A. J. Misquitta and K. Szalewicz, *J. Chem. Phys.*, **2005**, 122, 214109; b) J. García, R. Podeszwa, K. Szalewicz, *J. Chem. Phys.*, **2020**, 152, 184109.

- [39] E. I. Kim, S. Paliwal, C. S. Wilcox, *J. Am. Chem. Soc.* **1998**, *120*, 11192-11193.
- [40] R. A. Boto, F. Peccati, R. Laplaza, C. Quan, A. Carbone, J.-P. Piquemal, Y. Maday, J. Contreras-García, *J. Chem. Theory Comput.* **2020**, *16*, 4150-4158.
- [41] M. Spackman, E. Maslen. *J. Phys. Chem.* **1986**, *90*, 2020-2027.
- [42] A. M. Pendás, V. Luaña, L. Pueyo, E. Francisco, P. Mori-Sánchez. *J. Chem. Phys.* **2002**, *117*, 3, 1017-1023.
- [43] a) Gaussian 09, Revision C.01, M. J. Frisch, G. W. Trucks, H. B. Schlegel, G. E. Scuseria, M. A. Robb, J. R. Cheeseman, G. Scalmani, V. Barone, B. Mennucci, G. A. Petersson, H. Nakatsuji, M. Caricato, X. Li, H. P. Hratchian, A. F. Izmaylov, J. Bloino, G. Zheng, J. L. Sonnenberg, M. Hada, M. Ehara, K. Toyota, R. Fukuda, J. Hasegawa, M. Ishida, T. Nakajima, Y. Honda, O. Kitao, H. Nakai, T. Vreven, J. A. Montgomery, Jr.; , J. E. Peralta, F. Ogliaro, M. Bearpark, J. J. Heyd, E. Brothers, K. N. Kudin, V. N. Staroverov, R. Kobayashi, J. Normand, K. Raghavachari, A. Rendell, J. C. Burant, S. S. Iyengar, J. Tomasi, M. Cossi, N. Rega, N. J. Millam, M. Klene, J. E. Knox, J. B. Cross, V. Bakken, C. Adamo, J. Jaramillo, R. Gomperts, R. E. Stratmann, O. Yazyev, A. J. Austin, R. Cammi, C. Pomelli, J. W. Ochterski, R. L. Martin, K. Morokuma, V. G. Zakrzewski, G. A. Voth, P. Salvador, J. J. Dannenberg, S. Dapprich, A. D. Daniels, Ö. Farkas, J. B. Foresman, J. V. Ortiz, J. Cioslowski, D. J. Fox, Gaussian, Inc., Wallingford CT, 2010; b) D. G. A. Smith, L. A. Burns, A. C. Simmonett, R. M. Parrish, M. C. Schieber, R. Galvelis, P. Kraus, H. Kruse, R. D. Remigio, A. Alenaizan, A. M. James, S. Lehtola, J. P. Misiewicz, M. Scheurer, R. A. Shaw, J. B. Schriber, Y. Xie, Z. L. Glick, D. A. Sirianni, J. S. O'Brien, J. M. Waldrop, A. Kumar, E. G. Hohenstein, B. P. Pritchard, B. R. Brooks, H. F. SchaeferIII, A. Y. Sokolov, K. Patkowski, A. E. DePrincell, U. Bozkaya, R. A. King, F. A. Evangelista, J. M. Turney, T. D. Crawford and C. D. Sherrill, *J. Chem. Phys.* **2020**, *152*, 184108.

Table of Contents

Double hook-like molecule as PAH receptor. A new receptor prepared in a one-step reaction shows an excellent ability to bind PAH and exhibits interesting properties for developing sensors. Its behavior was thoroughly characterized with spectroscopic methods and rationalized with a thorough theoretical study. The image shows a UV/vis titration of PDI with perylene, presenting a colorimetric change.



Twitter

@bumabel

@nad_ro